AUSTIN AVENUE BRIDGES AT SAN GABRIEL RIVER
Condition Assessment and Evaluation

Georgetown, Texas 78626

Final Report
January 12, 2016
WJE No. 2015.5402

Prepared for:
Mr. David Lubitz, PE
Aguirre & Fields, LP
12708 Riata Vista Circle, Suite A-109
Austin, Texas 78727

Prepared by:
Wiss, Janney, Elstner Associates, Inc.
9511 North Lake Creek Parkway
Austin, Texas 78717
512.257.4800 tel | 512.219.9883 fax
Texas Registered Engineering Firm F-0093

AUSTIN AVENUE BRIDGES AT SAN GABRIEL RIVER
Condition Assessment and Evaluation

Georgetown, Texas 78626

Aaron Sterns, PE
Senior Associate and Project Manager

Sam Keske, PhD
Associate II

Brian D. Merrill, PE
Associate Principal

Final Report
January 12, 2016
WJE No. 2015.5402

Prepared for:
Mr. David Lubitz, PE
Aguirre & Fields, LP
12708 Riata Vista Circle, Suite A-109
Austin, Texas 78727

Prepared by:
Wiss, Janney, Elstner Associates, Inc.
9511 North Lake Creek Parkway
Austin, Texas 78717
512.257.4800 tel | 512.219.9883 fax
Texas Registered Engineering Firm F-0093

WJE ENGINEERS ARCHITECTS MATERIALS SCIENTISTS

TABLE OF CONTENTS

WJE ENGINEERS ARCHITECTS MATERIALS SCIENTISTS

AUSTIN AVENUE BRIDGES AT SAN GABRIEL RIVER
Condition Assessment and Evaluation

Georgetown, Texas 78626

INTRODUCTION

At the request of Aguirre & Fields, LP (A&F) and in accordance with our proposal dated October 1, 2015, Wiss, Janney, Elstner Associates, Inc. (WJE) has completed a forensic investigation of the Austin Avenue Bridges over the North San Gabriel River and South San Gabriel River in Georgetown, Texas. We understand that following a recent A&F structural review of the bridges, as reported in June 2014, the City of Georgetown requested additional forensic engineering investigation of the bridges to aid in the evaluation of bridge maintenance/repair/replacement options presented by A&F. The objective of our investigation was to gain an overall understanding of the existing condition of the bridges to aid in considering the potential bridge maintenance/repair/replacement options.

BACKGROUND

The bridges are of approximately the same vintage and construction and were completed in 1940. Each bridge has a total of seven spans and is constructed with a 7-inch concrete deck over nine longitudinal steel girders supported by concrete piers/abutments. Reference Figure 1 and Figure 2 for schematic orientation of the South and North Bridges, respectively. Substructure elements are referenced as numbered in the most recent bridge inspection report, in which each bridge contains Abutments 1 and 8, as well as piers adjacent to the San Gabriel River banks and bents supporting other spans. Each bridge contains four simply supported spans and a three-span cantilevered section consisting of cantilevered exterior spans and a suspended middle span. Spans are numbered from south to north within each bridge, including South Bridge Spans 1 through 7 and North Bridge Spans 1 through 7.

A thickened concrete sidewalk is cast integrally with the concrete deck; a steel handrail is also cast integrally with the deck. The concrete deck includes an approximately 2-inch thick asphalt overlay. Deck expansion joints are located at the ends of each span. The joints are located over substructure bearings except at cantilever spans. Additional deck construction joints are located at each intermediate diaphragm. The deck is not mechanically connected to the steel girders for composite action with the girders, but the deck bears on the girders and diaphragms, with deepened slab ribs at the diaphragms (Figure 3 and Figure 4). Diaphragms, supplemental bottom-flange plates, cantilever hinge mechanisms, and girder splices are typically constructed with riveted connections. The girders bear on ball-and-socket bearings consisting of a lead sheet between two curved steel plates (Figure 5 and Figure 6).

The bridges are currently load-posted for loads not to exceed 48,000 pounds gross weight or 21,000 pounds tandem-axle weight. We understand the posting was instituted based on conditions reported from a routine Texas Department of Transportation (TxDOT) bridge inspection completed in December 2013. Following A&F review, A&F presented options for maintenance/repair/replacement of the Austin Avenue Bridges to the City of Georgetown that range in scope from performing no work to complete bridge replacement, with complementary life-cycle cost analyses. To help assess the suitability of each option, WJE performed non-destructive and destructive testing of various bridge substructure and superstructure bridge elements, including the concrete foundations, steel girders, and concrete deck. WJE also reviewed the existing

documentation on the bridges, including recent reports and analyses and limited original construction documents.

DOCUMENT REVIEW

A&F provided the following documents for our review:

- Limited available construction drawings for the bridges, dated September 1938.
- The most recent Texas Department of Transportation bridge inspection record, with a supplemental load rating analysis, sealed by C. R. Barnhart, PE of Barnhart Constructors (Barnhart) on December 3, 2013.
- A letter from Barnhart to TxDOT, dated January 21, 2014, regarding the recommendation to load-post the North and South Bridges.
- The recent A&F bridge assessment report, dated June 5, 2014.

The original construction drawings were used as field data sheets while performing our field investigation. WJE reviewed the provided construction drawings, reports, and load rating analysis and noted the following pertinent information related to the existing bridge construction, condition, and rating:

- The drawings indicate the use of "Class A Concrete" for all substructure elements and the concrete deck. The original construction drawings do not indicate the grade of steel for deck reinforcement or for structural steel members but reference the 1938 State Highway Department of Texas Specifications.
- The AASHTO Manual for Bridge Evaluation [1] recommends using a value of 2,500 psi for compressive strength of sound concrete cast prior to 1959 and a steel yield strength of 33.0 ksi for structures built prior to 1954.
- Barnhart's December 2013 bridge inspection report and related letter to TxDOT indicated "advanced girder and deck support diaphragm top flange rust, directly under the concrete deck" and "severe pack rust on girder top flanges, being so pronounced as to have lifted the deck up from the top slab." The report indicated that the corrosion was most severe near the exterior girders, where sidewalk expansion joints were covered with metal plates and sidewalk construction joints were not sealed.
- The bridge inspection report and related letter recommended replacement of the bridge decks, with removal of girder and diaphragm corrosion, girder recoating, and installation of shear studs to create composite action between the girders and new concrete deck.
- The inspection included a "5" rating for the bridge superstructures, indicating "fair condition - minor deterioration of structural elements (extensive)" with a supplementary load rating analysis. The load rating analysis did not include a reduction in girder cross-section due to corrosion but indicated a reduced HS 15.9 load rating. We understand that bridge load postings were implemented to reflect the gross and tandem axle weights derived from that load rating analysis in accordance with TxDOT policies for off-system bridges.
- The A&F report concurred with the 2013 bridge inspection observations and load rating analysis. The report further indicated that girder bearing functionality has likely been compromised by bearing corrosion, as suggested by concrete spalling at vertical substructure faces adjacent to girder bearings.
- For a life-cycle cost analysis, the A&F report presents an assumed bridge replacement occurs after a remaining five year service life if repairs are not performed. The report indicates that short-term repairs, such as expansion joint replacement and recoating of steel girders, may extend the service life to 10 years, and replacement of the concrete deck may extend the service life to 20 years.
- The A&F report includes a life-cycle cost analysis, in which bridge replacement after 5 to 10 years appears to be the most cost-effective long-term method of achieving 75 years of service life.

FIELD INVESTIGATION

On November 2 through 6, 2015, Aaron Sterns, PE, Sam Keske, PhD, EIT, and Casey Jones, EIT, all of WJE, visited the site to conduct a limited condition assessment of the bridges, which included visual and delamination surveys, non-destructive evaluation of the configuration and cover depth of the in-place reinforcement, non-destructive evaluation of the member thicknesses of corroded and corrosion-free steel members, and material sampling as described herein.

Visual and Delamination Survey

WJE performed a visual survey of the bridges to document the existing conditions and extent of observed structural distress. WJE assessed all accessible, visible substructure and superstructure elements from ground level and also walked the topside of the bridges. WJE also completed an arm's length visual assessment of select structural elements using a 50-foot articulating boom lift (Figure 7). WJE performed mechanical sounding of accessible concrete elements to identify areas of concrete spalling or delamination. Observations related to each element are provided below.

Bridge Decks

1. The concrete deck had separated from the top of the outermost girder flanges by up to 3/16 inch at the north and south ends of the North Bridge. Form indentations were visible in the abutment back wall behind the deck at each separation, and expansion material between the deck and abutment back wall appeared to be compressed or partially dislodged (Figure 8). Minor surface corrosion was visible on the unpainted outer edges of the girder top flange, but no corrosion was visible at the top surface of the top flange, between the girders and deck (Figure 9). Figure 8 and Figure 9 were taken at the same location at the exterior of the westernmost girder at Abutment 1 of the North Bridge.
2. Isolated spalls with corroded reinforcement, totaling less than 50 square feet per bridge, were located at slab soffit locations in the North and South Bridges (Figure 10). Reinforcement clear cover at accessible spall locations was measured to be approximately 3/4 inch. The spalls were approximately 24 to 48 inches in diameter and represented less than 1 percent of the slab soffit area. Spall locations appeared random and varied relative to girder, span, or joint location.
3. Isolated spalls, generally without exposed reinforcement, were located at the chamfered haunch edges of many locations at both bridges (Figure 11). The spalls were more common along the outer face of the outermost girders, especially at span ends.
4. The concrete infill at many diaphragms exhibited cracking up to 1/16 inch in width, including at locations exhibiting minimal corrosion formation (Figure 12). The cracking generally originated at reentrant corners formed where the concrete was cast adjacent to girder top flanges. Based on the original construction drawings (Figure 3), the infill contains longitudinal steel reinforcement that terminates near the girder webs and transverse, vertical reinforcement that extends into the deck. Figure 12 was taken on the interior side of the girder shown in Figure 8 and Figure 9.
5. During a rain event on November 5th, water leakage from the bridge decks was observed at several piers/bents, especially near the outermost girders (Figure 13). Considering the previous A&F report and based on the widespread extent of the condition, WJE did not identify specific joint leakage locations.
6. Based on review of the original construction drawings, the original pedestrian railings remain in place at the North and South Bridges. Coatings at the pedestrian railings were generally intact, and the railings did not exhibit apparent corrosion or vehicular impact damage. The deck soffit exhibited minor surface

corrosion staining beneath some railing posts, where the posts were cast integrally with the deck. A spall exposing a corroded post base was visible in at least one location (Figure 14).

Steel Superstructure

7. Girder webs typically exhibited moderate corrosion section loss near diaphragm connections at exterior girders and minor pitting or surface corrosion at interior diaphragm connections. The corrosion was typically concentrated where concrete diaphragm infill is cast flush with the adjacent girder web (Figure 15). Coatings appeared to have been applied to the girders near the corroded connections, but with limited functionality (paint bubbling or flaking) due to corrosion product expansion.
8. Expansive corrosion product appeared to be confined between the concrete infill and diaphragm top flanges between the outermost girders of both bridges, a condition known as "pack rust." Some diaphragm top flange tips exhibited total corrosion section loss (Figure 16). Diaphragm bottom flanges at these locations typically exhibited minor to moderate corrosion section loss. Interior diaphragms generally exhibited minor corrosion section loss or surface corrosion.
9. Away from diaphragm connections, steel girders generally exhibited light surface corrosion or no visible corrosion. No evidence of pack rust formation was observed at the interface between the concrete deck and the girders.
10. WJE observed South Bridge Span 3 and North Bridge Span 5, which span the branches of the San Gabriel River, from ground level at adjacent riverbanks. No atypical corrosion or discoloration was apparent at suspended span bearings or girder-deck interfaces.

Bearings and Substructures

11. Consistent with the A&F report, most steel plate bearings exhibited minor corrosion and deterioration of lead sheets between steel bearing plates (Figure 17). Isolated bearings at exterior girders exhibited moderate corrosion and pack rust (Figure 18).
12. The concrete beneath the bearing at South Bridge Bent 2 exhibited a large spall (Figure 19). Intact portions of the spalled concrete exhibited concrete cover of up to 2 inches (Figure 20). A similar, large insipient spall was located at South Bridge Abutment 1 (Figure 21).
13. Isolated spalls or insipient spalls were identified at abutments, bents, and piers. Such spalls were somewhat more common at abutments than at bents/piers. Some of the spalls exhibited shallow cover over corroded reinforcement (Figure 22 and Figure 23).
14. Substructure elements exhibited widespread organic staining beneath expansion joints, and the south end of the North Bridge exhibited widespread organic growth attached to the substructures.
15. The east end of the Pier 3 of South Bridge exhibited up to 24 inches of scour beyond the top of the pier footing (Figure 24). By comparison, A&F Report Photograph 25 appears to illustrate up to 21 inches of scour beyond the top of that pier footing, which is generally consistent with our observations. Boulders and debris nearby in the San Gabriel River appeared to redirect a disproportionate volume of water toward that corner.

Non-destructive Structural Survey

At accessible spall locations, the former concrete clear cover was estimated by measuring the projected cover from the concrete surface adjacent to the spall. At selected locations of the concrete deck soffit, bents, and abutments, concrete cover depth and reinforcement spacing were determined non-destructively using ground-penetrating radar (GPR) equipment. In general, GPR equipment does not perform well in the vicinity of delaminations or other visible concrete deterioration. Thus, reinforcement cover depth was

measured visually at typical locations exhibiting spalling with exposed reinforcement, and GPR measurements were obtained at representative locations that did not exhibit apparent distress.

The reinforcement locations and cover depths were recorded using GPR in the field and processed using software licensed from the GPR manufacturer (Figure 25). For comparison, Figure 26 illustrates the distribution of cover from all scans of the deck soffit. To calibrate and confirm the GPR results, cover depth was measured directly by drilling into the concrete at discrete bar locations. Table 1 summarizes the results of our limited GPR cover depth assessment. In the table, cover depths are combined for the two bridges, as cover depths were generally consistent. In general, reinforcement spacing corresponded to details shown in the original construction drawings or was narrower than that shown in the drawings. Based on observations of reinforcement exposed by spalls, as well as two samples obtained from the bridge deck, reinforcement appeared to be of the size shown in the original construction drawings.

WJE measured the thickness of steel superstructure members using ultrasonic thickness (UT) testing equipment. The UT equipment calibration was verified at several representative elements with a caliper. In general, girder top and bottom flanges, as well as diaphragm webs, exhibited minor to no measureable section loss. Girder web thickness at isolated diaphragm connection locations, typically within the outermost two girders, was reduced by up to 3/16 inch, or 30 percent. However, the corrosion was isolated to the portion of the web adjacent to the concrete infill, representing a net web loss of approximately 10 percent. Isolated diaphragms, typically between the outermost two girders, exhibited complete section loss at flange tips and up to 5/16 inch, or up to 60 percent, section loss at bottom flanges. Diaphragm flanges between interior girders typically exhibited moderate to no corrosion section loss.

Field Carbonation Testing and Material Sampling

The depth of carbonation was tested by applying a phenolphthalein indicator solution into the drilled holes that were used to verify reinforcement cover depth (Figure 27). Phenolphthalein induces a pink color on the surface of the concrete if the concrete has a pH greater than 9. A treated area of the concrete that does not undergo a color change has a pH below 9 and is considered fully carbonated. The distance from the exterior surface of the reinforced concrete elements to the color change boundary was measured in the field to determine approximate carbonation depth. Because the protective passive layer on the reinforcing steel may be compromised when concrete pH is 9.5 to 11, carbonation-induced corrosion may initiate at slightly greater depths than the carbonation front indicated by phenolphthalein testing. Field measurements of carbonation at various concrete elements are presented in Table 2.

WJE extracted 3-3/4-inch diameter concrete cores from various concrete elements of each bridge for laboratory investigation as described in the following section. WJE obtained seven cores from each bridge: two from each deck (Figure 28), two from representative piers/bents exhibiting apparent surface staining, two from representative piers/bents exhibiting little to no apparent surface staining (Figure 29), and one additional sample representing ancillary structures or atypical conditions. Figure 30 is an overall view of the samples collected. Cores from the concrete deck penetrated through the full depth of the deck, including the asphalt topping. Cores from other concrete elements typically exhibited lengths of at least double the core diameter (7-1/2 inches), such that samples extended well beyond the outermost layer of steel reinforcement and were suitable for compressive strength evaluation.

WJE cored through single reinforcing bars in two of the deck cores, Cores 6 and 8 (Figure 31 and Figure 32). Reinforcement in Core 8 exhibited no corrosion, while the reinforcement in Core 6 exhibited minor surface corrosion (Figure 33). Carbonation testing of the two cores indicated that the carbonation front extended to

a depth of 1-1/2 inches in Core 6 and 7/8 inch in Core 8. Concrete cover was approximately 1-1/4 inches in both cores. Section loss of the corroded bar in Core 6 was estimated to be less than 3 mils, which is equivalent to 0.5 percent of the No. 5 bar diameter.

LABORATORY ANALYSES

Of the fourteen cores WJE obtained from the Austin Avenue Bridges, the following tests were conducted on representative groups of cores:

- Compressive strength testing of two deck cores and two substructure cores.
- Acid-soluble chloride content testing of ten cores, at several discrete depths within each core (thirty-six samples total), to determine chloride concentrations up to the depth of the deck and substructure reinforcement.
- Petrographic examination of two cores to characterize the general composition and quality of the deck and substructure elements.
- Carbonation testing of remaining samples.

Cores for carbonation, chloride, and petrographic examination were cut longitudinally using a diamond-bladed rock saw so multiple tests could be performed on a single core. The concrete cores were prepared for all tests in the WJE Austin Laboratory; chloride specimens were then shipped to a third-party testing agency. The identification, locations, and testing protocol for the cores are given in Table 3. Results of the laboratory analyses are further described in the following sections.

Compressive Strength Testing

Compressive strength testing was performed in accordance with ASTM C42, *Standard Test Method for Obtaining and Testing Drilled Cores and Sawed Beams of Concrete*. The cores were trimmed to length and sealed for 5 days in plastic bags to allow moisture conditioning prior to capping and testing in compression. Compressive strength results are included in Table 3. The measured compressive strengths ranged from a low of 4,790 psi for Core 7 to a high of 7,000 psi for Core 12. The difference between pairs was not statistically significant at the 90th percentile. The overall average compressive strength of the four cores was 5,850 psi.

Carbonation Testing

Immediately upon cutting the cylinders into parallel samples for chloride testing and petrographic examination, phenolphthalein indicator was applied to all samples not required for those tests. WJE then determined an approximate carbonation depth for each core sample (Figure 34). Summary results are presented in Table 2. The results generally agree with the field carbonation testing results, indicating relatively less significant carbonation at substructure elements than the deck soffits, with greater than 1 inch of carbonation at the concrete deck soffit. Carbonation results are reviewed with respect to service life modeling in a later section.

Chloride Analysis

Ten core specimens were selected for acid-soluble chloride analysis in accordance with ASTM C1152, *Standard Test Method for Acid-Soluble Chloride in Mortar and Concrete*. Discrete regions of each sample were ground to a powder for acid-soluble chloride testing. Three 1/2-inch regions of concrete from substructure elements were tested: a region near the exterior concrete surface, a region corresponding to the average cover depth to the substructure elements, and a region approximately halfway between the other

regions. Six 1/4-inch regions of concrete from the bridge decks were tested, because relatively greater chloride exposure was possible at these elements and the deck typically exhibited less concrete cover to the reinforcement.

A lower-bound threshold for initiation of corrosion of uncoated steel reinforcement is considered to be approximately 0.20 percent chloride by weight of cement in non-carbonated concrete [2]. The threshold chloride content in carbonated concrete is generally lower, but difficult to define, as the corrosion-inducing effects of chloride ingress are synergistic with carbonation—corrosion is more likely when both occur in concrete, beyond what would be expected from one mechanism alone. Based on the unit weight of the concrete and an estimate of cement content derived from the petrographic examination described below, chloride ion concentration was compared to percent by weight of concrete, in which a chloride corrosion threshold value of 0.025 percent chloride ion by weight of concrete equates to approximately 0.20 percent chloride by weight of cement. Based on the material testing performed, the chloride contents were less than 0.022 percent chloride ion by weight of concrete in substructure elements and less than 0.027 percent in the bridge decks, at the average depth of the reinforcement. The results are summarized in Table 4.

Petrographic Examination

Petrographic examination based on ASTM C856, *Standard Practice for Petrographic Examination of Hardened Concrete*, was performed by WJE for two core samples obtained by cutting a representative deck core and substructure core. One saw-cut surface from each core was lapped with progressively finer grinding media. They were then examined using a stereomicroscope at magnifications up to 160X (Figure 35). The samples were similar in composition and mix proportions. The petrographic findings are as follows:

The coarse aggregate was uncrushed, predominantly limestone gravel having a nominal maximum size of approximately 3/4 inch. The fine aggregate was natural sand containing major amounts of limestone, quartz, and chert. The aggregates were sound, well graded, and uniformly distributed. The aggregates were tightly bonded to the paste.

The paste was gray to light gray, uniform, hard, and had a semiconchoidal granular texture. No supplementary cementitious materials, such as fly ash, slag cement, or silica fume, were observed. Calcium hydroxide crystals from the cement hydration were moderate in size and abundant in concentration. The cement hydration appeared to be normal for the age of the concrete, indicating advanced hydration. The compositional and textural characteristics of the paste indicated that the concrete had a moderately high water-to-cement ratio (w/cm), estimated to be in the range of 0.45 to 0.53 for both samples. The portland cement content was estimated to be approximately 500 pounds per cubic yard.

The concrete was non-air-entrained, with a total air content estimated to be 1 to 2 percent for both cores. Voids were mostly coarse and irregular, consistent with entrapped air voids. Voids were uniformly distributed and free of enclosed contaminants. No distress mechanisms were apparent in the paste, aggregate, or paste-aggregate interface transition zone.

DISCUSSION

Element Condition

Concrete Deck

The concrete distress observed in the reinforced concrete deck appears to be associated with two mechanisms—1) corrosion of the embedded steel reinforcement, and 2) deck detailing at concrete-to-steel joints. Based on our limited condition assessment, corrosion of the reinforcement appears to have occurred where carbonation has progressed beyond the depth of concrete cover at the shallowest reinforcement. Chloride-induced corrosion, usually due to salt or other chloride exposure, is unlikely within non-carbonated regions of the concrete, considering the results of the laboratory chloride analysis and observed service conditions.

Carbonation, which occurs over many years, reduces concrete's protection of embedded steel reinforcement. It is a chemical change that reduces the naturally high pH (alkalinity) of concrete over time due to exposure to carbon dioxide in the atmosphere. The high pH of the concrete, typically around 13, causes a passive oxide layer to form at the embedded reinforcing steel, thus protecting the steel from corrosion. Once the depth of carbonation reaches the reinforcement, the steel loses its passivity and will start to corrode with exposure to sufficient amounts of moisture and oxygen. If the pH of the concrete drops below 11, the passive layer can be compromised. Carbonation progression is influenced by moisture and relative humidity (RH), surface finish and coatings, cement composition, permeability of the concrete, and the availability of carbon dioxide.

Based on the phenolphthalein testing performed, the depth of carbonation at the deck soffits averages slightly less than one inch. The carbonation depth is likely greater at areas near cracking, delamination, or spalling. Any cracking will further serve to increase the rate of carbonation and associated corrosion. As indicated by the limited testing, comparison to Table 2, and evidence of spalls primarily at locations of shallow cover, full carbonation has likely reached the slab soffit locations of shallowest cover and resulted in the observed concrete spalling with exposed, corroded reinforcement. The penetration rate of carbonation generally occurs at a logarithmic rate versus depth, essentially slowing as time increases. Therefore, additional considerations of reinforcement depth variability and other material factors is necessary to reasonably estimate the rate of future carbonation-induced distress. Such considerations are discussed in the following section on service life modeling.

Observed delaminations and spalls likely originated at locations with the least concrete cover, other substrate defects such as cracking or other mechanical damage, or areas with locally poorer quality concrete, due to the exterior exposure and effects of carbonation. In general, the spalling and delaminations appear to be relatively small in area and randomly distributed at slab soffit locations. However, the iron oxide formed as a result of corrosion is expansive. Once corrosion of the reinforcement initiates, corrosion continues to propagate until surface damage manifests, which further serves to remove the corrosion protection provided by the concrete. Accordingly, once corrosion becomes visually apparent in concrete structures, corrosion formation at exposed reinforcement typically accelerates.

Modern detailing typically avoids creating construction conditions that may induce tension in unreinforced concrete elements. The unreinforced, chamfered edges of concrete haunches cast adjacent to girder top flanges (Figure 36) are subject to tension as a result of thermal or load-induced deck movement or expansive corrosion of the outer edge of the top girder flange. Spalling of the unreinforced concrete toe is likely in such circumstances, even if the concrete material is sound. Still, the chamfered toe has minimal structural

significance, so spalling does not present a risk to structural integrity of the bridges. Considering the lack of exposed, corroded reinforcement or significant girder corrosion at the majority of chamfer spalls, the distress is likely related to poor detailing instead of structural overloading or girder corrosion formation.

Crack formation in the concrete infill above steel diaphragms likely resulted from poor detailing of the diaphragms combined with any movement of the steel superstructure relative to the deck. Because the deck does not act compositely with the steel girders, any differential movement of the deck relative to the girders likely induced tension in the infill cast beneath the top girder flange. Crack formation should not significantly affect the compressive load-bearing capability of the concrete infill, and the concrete contributes little to the lateral bracing provided by the steel diaphragms. Therefore, the cracks do not present a risk to the structural integrity of the bridges, although they may create falling debris hazards over time.

Separation of the concrete deck from the top flange of the outermost girders at the ends of the North Bridge was most likely caused by unintended binding between the abutment back walls and the longitudinal ends of the deck. An expansion board was installed between each deck end and abutment back wall, but indentations in the back wall and visible compression of the expansion board near the outer deck edges suggest that the deck is bearing on the abutment walls instead of the girders at these locations. Because the deck is not mechanically anchored to the steel girders below, separation of the deck from the girders may not induce structural distress in either component. The deck does not exhibit apparent cracking or other distress at these locations, other than the spalling of the unreinforced, chamfered haunch edges as discussed earlier, indicating that the condition does not present an immediate structural concern. Furthermore, pack rust typically initiates at unconfined member edges and propagates inward. Lack of corrosion at the top flange exterior edges of the exposed girders suggests that the deck separation is not related to formation of pack rust between the girders and deck. The diaphragm crack indicated in Figure 12 appears to be the result of this lifting of the deck off of the girder top flange as indicated in Figure 8 and Figure 9.

Although the current condition of the concrete deck generally does not indicate reduced structural integrity of the bridges, ongoing corrosion and associated deterioration, as well as chamfered haunch spalling, will likely continue over time. Formation of additional slab soffit concrete spalls will present a safety concern for falling debris. A service life model predicting the extent of spall formations in response to reinforcement corrosion is presented in the following section. Minor spalling of chamfered haunches is also likely to continue, which also presents a safety concern for falling debris.

Steel Members

Corrosion of the steel girders and diaphragms is generally limited to locations exposed to repeated moisture exposure—unsealed deck construction joints and expansion joints. Based on the limited original construction drawings, deck slab construction joints were intentionally located over each intermediate diaphragm. Details indicate installation of a steel plate divider at each construction joint (reference A&F Report Figure 3), which likely causes the joints to act similarly to cracks, providing a route for moisture infiltration to the steel diaphragms and girders below. While the later addition of an asphalt topping appears to have limited the moisture infiltration at interior girders and diaphragms, the un-topped concrete sidewalk cast integrally with the deck remains unsealed, thus permitting repeated moisture exposure to the outermost girders and diaphragms. Similarly, while expansion joints between spans include waterproofing sealant joints, the joints do not appear to be performing as intended, likely due to long-term deterioration.

Alignment of construction joints over intermediate diaphragms, and the use of girder and diaphragm top flanges as stay-in-place forms, likely exacerbated the corrosion of the diaphragm top flanges. It is unclear

if the steel members were coated before concrete was cast flush with them, but concrete prevents any coating reapplication. The reported recoating of exposed steel member surfaces has likely significantly reduced the rate of corrosion propagation globally, but concentrations of pack rust at diaphragm top flanges will likely continue if construction joints and expansion joints are not sealed (or resealed). In our experience, such pack rust is likely to buckle the intermediate diaphragms before inducing apparent distress in the adjacent concrete deck or girders. However, corrosion products tend to retain moisture, which is likely to cause isolated corrosion section loss of girder webs at diaphragm connections.

Girders typically only exhibited measurable corrosive section loss at diaphragm connections. The loss appears to be concentrated at the web, while top and bottom girder flanges typically exhibit little to no surface corrosion. The web section loss is unlikely to present an immediate risk to the structural integrity of the girders, as the corrosion is typically located at regions of relatively small shear demand. However, corrosion of the connections is expected to propagate at an increasing rate due to the moisture retentive nature of corrosion product. Corrosive section loss may create a falling debris hazard unless corrosion is completely removed and a corrosion-inhibiting coating is applied at locations susceptible to corrosion.

Bearings and Substructures

Concrete substructures generally exhibit very minor corrosion distress. The lack of distress, despite the potential for carbonation as discussed earlier regarding the bridge decks, is likely attributable to the comparatively deep concrete cover measured at all tested substructure elements and lack of corrosive environmental exposure (deicing salts, marine environment, etc.). All tested bent/pier elements exhibited concrete cover to the reinforcement of at least 1-3/4 inches, with average cover of approximately 2-1/4 inches. This amount of concrete cover is consistent with modern construction provisions [3], although the bridges predate these provisions.

Isolated substructure distress near bearing caps is likely related to deterioration of the girder bearings, as previously indicated in the A&F report. Furthermore, the random location of the concrete distress suggests that other defects, such as cracking, randomly shallow reinforcement, or mechanical damage, likely contributed to the observed spalling distress. The observed spalling appears to have predominantly affected the outermost layer of reinforcement—stirrups near the distress—with limited to no deterioration of the longitudinal substructure steel. The bearing capacity of the third girder from the east of South Bridge Span 2 may be affected by the distress, as previously noted by A&F. Considering the distribution of loading through the deck to adjacent girders, the reduced bearing capacity of the girder should not present an immediate structural integrity hazard. However, restoration of that bearing will likely require temporary jacking/shoring of the bridge and partial-depth concrete repair.

Corrosion accumulation or lead sheet deterioration in the steel girder bearings likely contributed to the isolated occurrences of concrete substructure spalling by reducing the ease of movement of the steel bearings. Furthermore, as lead sheets within the steel ball-and-socket bearings deteriorate or become partially dislodged, the total thickness of the bearing is reduced, thus potentially resulting in the observed separation of the deck from the girders at the ends of the North Bridge. Deterioration of the lead padding should not present an immediate structural capacity hazard. However, degradation of the lead padding should be expected to continue if not addressed in conjunction with partial-depth concrete bearing repairs and improvement of construction and expansion joint sealants. In current bridge maintenance practice, lead-padded steel bearing assemblies are typically replaced with neoprene bearing pads upon deterioration. Neoprene bearing pads reduce the transmission of dynamic live-load impacts to substructure elements and

increase the translational capacity of the bearings, thereby improving the long-term durability of the substructure bearing elements.

Service Life Modeling for Concrete Corrosion

Approach

Service life in a given setting must be defined based on requirements unique to that structure in terms of performance and occupancy needs. The service life for the Austin Avenue Bridges depends upon the intended function of the structure and requirements of the owner, the City of Georgetown. The end of service life may be defined by various parameters, including:

- Reduction of the bridge structural capacity, relative to the original load capacity or a given load rating.
- Reduction in drivability resulting from development of deck potholes or spalling.
- Reduction in serviceability resulting from distress that presents a falling debris hazard or aesthetic concern.

The specific amount of deterioration that can be tolerated varies by element type, and elements may be designed for differing service durations depending upon the ease of replacement. The distress mechanisms leading to deterioration and the methods by which further deterioration would be mitigated must also be considered for efficient evaluation of remaining service life. In this structure, deterioration of the concrete due to carbonation is most likely to control the service life of the bridge, particularly regarding carbonation at the deck soffit. Existing corrosion of the steel girders and diaphragms appears unlikely to significantly affect capacity of the bridge at this time. Therefore, mitigation of the primary superstructure corrosion mechanism—leakage at the intermediate diaphragms—and proper cleaning and recoating of corroded girder and diaphragm locations should distinctly prolong the service life of the steel superstructure. Prediction of future steel-member service life after coating reapplication is then relatively straightforward and is a function of coating durability and maintenance.

Corrosion of the reinforcing bars in the concrete is likely to be the most financially demanding deterioration mechanism to mitigate in the Austin Avenue Bridge, based on the relative volume of aging concrete. The current corrosion appears to be predominantly related to carbonation, as minimal chlorides were present in various elements. Based on the depth of reinforcement, carbonation will affect the deck soffit disproportionately sooner than it will affect the concrete substructures. Resulting corrosion of the deck is likely to create falling debris hazards in the form of concrete spalls, generally with limited reduction of bridge structural capacity. Carbonation is generally a very slow-acting corrosion mechanism, so formation of falling debris hazards is likely to be very gradual. This is evidenced by the relatively minor extent of soffit spalling observed in our recent field investigation. Service life modeling of concrete corrosion is therefore a valuable tool in predicting the time until which implementation of deck repairs or replacement may become necessary.

Basis for Corrosion Model

Corrosion-related damage to concrete generally occurs in two stages: 1) time elapsed between concrete construction and when environmental factors change the concrete material to allow corrosion of embedded reinforcement to begin, i.e. initiation time (t_i); and 2) time elapsed between when corrosion begins and when build-up of corrosion product exceeds the threshold volume needed to crack or spall the concrete and result in surface damage, i.e. propagation time (t_p). This concept is illustrated in Figure 37 and forms the basis for the service life models developed for the Austin Avenue Bridges.

The two-stage damage formation concept can be applied to concrete experiencing corrosion-related damage by considering the sequence that leads to delamination and spalling. For a single bar location undergoing carbonation-induced corrosion, this includes the following steps, as illustrated in Figure 38:

- First, initially after construction, the bar is embedded in young concrete and is passivated against corrosion.
- Second, concrete carbonation proceeds from the exterior surface.
- Third, after much time has passed, the carbonation front reaches the bar and changes the pH at the bar surface. Corrosion initiates at the surface of the bar closest to the exposed face of the concrete element.
- Fourth, carbonation proceeds deeper into the concrete, and corrosion propagates around the bar.
- Fifth, corrosion products on the bar builds up to a sufficient level to cause cracking, delaminations, or spalls in the concrete that become detectable from the surface.

An established probabilistic modeling approach developed by Sagüés [4] was adapted and used as the basis for the Austin Avenue Bridge service life models. The model determines the amount of surface area of the structural element that is affected by corrosion based on statistical distributions of key parameters considered to govern corrosion initiation. It recognizes the fact that corrosion is a local process that develops at multiple locations over time depending on the local propensity for corrosion. Time to damage formation is considered as a probabilistic variable influenced by combinations of independent random variables. In this analysis, the independent random variables include concrete cover depth, carbonation rate, and corrosion rate. To determine the time until damage occurs, a randomly sampled cover depth is paired with a randomly sampled rate of carbonation to determine t_i. Upon corrosion initiation, a randomly sampled rate of corrosion is paired with a maximum permissible amount of corrosion to determine t_p. Time until damage, t_d, equals the sum of t_i and t_p.

After estimating the time to corrosion initiation or damage with respect to a single location (bar), the probability of corrosion initiation or damage at that location can be extrapolated to the performance of the structural element as a whole (surrounding slab). If the structural element is of sufficient size for multiple, independent locations of corrosion-related damage to develop (entire deck), it can be discretized into a large number of segments with properties defined by statistical distributions that are measured or assumed. The cumulative probability of the slab structural element exhibiting corrosion initiation or damage through a given time then can be used to predict the percent area of the deck where corrosion has initiated or resulted in damage over time.

Model Considerations

Table 5 summarizes the model input parameters utilized in the Austin Avenue Bridges service life models. The distribution for concrete cover was modeled based on the depths measured by GPR scans in the field (Figure 26). A lognormal distribution was used, since this type of distribution reasonably described the data set and is well suited to describing datasets in which values are close to but greater than zero. An equivalent cover was defined within the model, using the centroid of the semi-circular arc for the near-surface half of the bar, to account for the time elapsed between when the carbonation front passes from the leading edge to the center of the bar.

Carbonation rates are ultimately dependent on a wide range of factors, which include: variations in concrete relative humidity, carbon dioxide concentration of the air, cement chemistry, concrete mix parameters - primarily permeability, surface finishes, and local defects. Because the time history and appropriate values

for many of these properties are unknown, a common model for quantifying carbonation rates from Parrott [5] was chosen.

$$carbonation\ depth\ (t) = A\sqrt{t}$$

Where:
A is a constant determined based on field or laboratory carbonation depth measurements, and
t is time since construction.

After corrosion initiates, corrosion product builds up until a crack propagates to the concrete surface, or a delamination or spall is caused in the surrounding concrete. The propagation time until damage formation is dependent on: cover depth, properties of the concrete and of the steel-concrete interface, type of corrosion products, size of reinforcing, and corrosion rate. Furthermore, the corrosion rate in carbonated concrete is strongly correlated to the RH of the concrete. Therefore, a probabilistic corrosion rate should be considered. In the absence of RH data for the Austin Avenue Bridges, two corrosion rates agglomerated from the literature [6 – 10] were considered in order to bracket the likely range of behavior—a relatively slower rate corresponding to 70 percent RH, and a relatively faster rate corresponding to 90 percent RH. For reference, the average daily RH in the Georgetown area is approximately 67 percent.

Propagation time until damage formation is influenced by the rate of corrosion and the geometry and the physical properties of the concrete and reinforcing bar. A constant threshold corrosion section loss of 3 mils was selected based on WJE's experience with corrosion-induced damage in structures of similar vintage and construction.

Modeling Results and Discussion

Service life modeling was conducted to assist in budgeting and scheduling of appropriate repair or maintenance strategies. The models do not consider the effect of atypical or localized features, e.g. pedestrian rail posts, leaking joints, etc., that may promote localized deterioration, so results should only be considered an estimate of general conditions. Also, considering the assumptions and simplifications incorporated, estimates should be considered accurate to ± 5 to 10 years, with a prediction horizon of approximately 50 years. Achievement of increased precision or a greater prediction horizon would require more thorough material sampling and field testing. From review of Table 2, and use of Parrot's carbonation estimate [5], carbonation is unlikely to significantly affect substructure reinforcement within the predictable future. Therefore, service life modeling was only performed for the deck soffit concrete, where carbonation has already begun to reach the depth of the deck reinforcement.

Based on measured carbonation rates and concrete cover depths, the carbonation front has likely reached approximately 20 percent of the deck soffit bottom reinforcement layer (Figure 39). Even if future carbonation-induced corrosion propagation is relatively gradual, the extent of carbonation is significant and is likely to limit the future service life of the decks, unless mitigation strategies are implemented. As previously discussed, damage from carbonation-induced corrosion can be difficult to predict considering the limited amount of visible damage and relatively limited destructive testing of corroded reinforcement conducted by WJE. Figure 40 presents time to damage formation, assuming corrosion rates associated with relatively rapid (higher RH) and gradual (lower RH) corrosion rates derived from the literature.

Figure 40 illustrates that, at a relatively high RH of approximately 90 percent, internal corrosion propagation at carbonated concrete regions would likely have already resulted in relatively broad surface

distress. By comparison to actual damage rates observed during our field investigation, the approximate corrosion rate is likely more similar to those observed in concrete approaching 70 percent RH.

Based on the slower corrosion propagation rate, carbonation-induced corrosion is likely to result in visible damage to approximately 10 percent of the deck soffit within the next 30 to 50 years. However, considering the combined area of exposed deck soffit, approximately 33,000 square feet, spalls at 10 percent of the North and South Bridges represent approximately 3,300 square feet of visible distress. Therefore, a more conservative limit for deck service life may be warranted to limit the propagation of falling debris hazards. For example, even the relatively gradual propagation model indicates damage formation at approximately 1,000 square feet of deck soffit within the next 30 years, based on current exposure conditions. That model also predicts the current extent of visible damage (approximately 1 percent) to double approximately every 6 years, in the absence of corrective measures.

Bridge Inspection and Load Rating

Based on the most recent Bridge Inspection Report and accompanying letter to TxDOT, the superstructures of the North and South Bridges were assigned a component condition rating (CR) of, "5 - Fair Condition," indicating widespread, or extensive, minor deterioration of structural elements. Commentary to the inspection report indicates that the main steel members were rated "5" because of severe pack rust formation at the top flange. Meanwhile, the secondary members (diaphragms) and connections were rated "6" to "8," in which a "6" rating indicates, "Satisfactory condition - minor deterioration of structural elements (limited)." According to TxDOT inspection practices for off-system bridges (not owned by the State of Texas), application of a CR of "5" requires analysis of the bridge's load capacity, or load rating, with posting of a bridge based on the Inventory Rating (IR) if the IR is less than the HS 20 standard bridge load. The IR represents the live load that can safely utilize the bridge for an indefinite period of time. The bridge load capacity needs not be posted, regardless of the inspection rating, if the IR is greater than HS 20. Per TxDOT policies, if the CR is "6" or higher, the resulting load-posting is to be based on the Operating Rating (OR) which in this case exceeds HS-20 - meaning that the bridge would not be load-posted.

The National Highway Institute (NHI), which nationally standardizes the bridge inspection rating system and trains inspectors, acknowledges that, because bridge inspection ratings are subjective in nature, inspection ratings are permitted to differ by ± 1 between inspectors. For example, a bridge rated "5" by one inspector may be rated "6" by another inspector. Considering the implications of application of a "5" rating to the Austin Avenue Bridges and the additional, advanced inspection and service life modeling techniques applied during this investigation, the assigned inspection rating warrants further consideration.

In his letter to TxDOT, Mr. Barnhart noted that the gaps observed between some girder ends and concrete decking is likely due to pronounced formation of pack rust between the deck and girders. Based on our review of the construction documents and our site investigation, the gaps were more likely caused by flattening of the lead sheets within steel bearing assemblies and other potential settlement mechanisms including mechanical damage of the concrete under the steel plate bearings. As the girders dropped slightly over time, the deck likely began to bear against the abutment back wall and did not settle uniformly with the girders. Based on the absence of identifiable pack rust on *primary* girder elements, lack of apparent corrosion at the visible girder-to-deck gaps, and evidence of binding between the deck end and abutment back wall, pack rust formation at girder top flanges appears highly unlikely. While corrosion formation at diaphragm connections has somewhat reduced the net web area at discrete girder locations, the affected regions are exposed to relatively little shear, the primary load resisted by the webs. Therefore, in the absence of widespread structurally significant primary member deterioration, modification of the primary structural

member rating to a "6" may be warranted, although we understand from discussions with TxDOT that raising a condition rating is unlikely and not a preferred approach.

Pack rust formation at *secondary* steel diaphragms is unlikely to result in deck separation or reduction in bridge integrity. The relatively less stiff diaphragms are likely to buckle due to pack rust formation before inducing uplift in the deck. The buckling or deterioration of such diaphragms is unsightly and may present a falling debris hazard over time. While the condition of the diaphragms does not currently appear to affect structural integrity, diaphragm degradation may eventually affect the performance of the bridges.

While the completed structural analysis indicates that the IR is less than HS 20, we understand that a primary concern regarding the load-carrying capacity of the in-place bridge involves the perceived limitation of emergency vehicle (fire department) accessibility. Based on Texas Transportation Code, Title 7, Subtitle E, Section 622.952, vehicles owned or operated by public, private, or volunteer fire departments are exempt from the load-posting currently in place at the bridges. Therefore, no additional action is required for such vehicles to utilize the bridges. However, additional analysis modifications may also be warranted based on the additional investigation and observed conditions, if seeking to restore un-posted HS 20 load-carrying capacity. Analysis modifications that may be warranted, depending upon the details of the existing analysis, include:

- Increase of deck concrete compressive strength, from 2,500 psi to 4,500 psi, to reflect the results of core cylinder compressive strength testing.
- Refined load distribution for determining live load response, based on finite element modeling of the deck-girder system.
- Fully braced positive flexural analysis, based on the above discussion regarding chamfered deck haunch encapsulation of the girder top flanges.

POTENTIAL BRIDGE MAINTENANCE STRATEGIES

Based on the observed condition of the bridges, the results of our laboratory analyses, and the predictions from bridge-deck service life modeling, the Austin Avenue Bridges appear to be capable of remaining in service for an extended duration if proper maintenance strategies are implemented. To maintain the bridges in a minimally-serviceable condition, the following potential bridge maintenance strategies are presented for consideration:

- Continued maintenance inspections in addition to the currently utilized routine TxDOT in-service safety inspections of the bridges. Conditions observed during our site investigation, such as separation of non-composite girders from the deck above, do not appear to have developed suddenly or present an imminent hazard to structural integrity. However, routine inspection would provide points of comparison to monitor the development of bridge hazards over time.
- Periodic hammer-sounding or physical examination of concrete spall locations or potential spall locations that may present falling debris hazards, including locations with excessive cracking, loose concrete, or concrete corrosion staining. The rate of carbonation-induced corrosion formation is expected to accelerate over time, resulting in more apparent distress in the next 15 to 30 years. Non-structural chamfered concrete haunches are also likely to develop spalls that present a falling-debris hazard due to their configuration, even if not directly affected by carbonation and internal reinforcement corrosion. Periodic examination of concrete spall and potential spall locations could be completed in conjunction with routine in-service visual inspections or at other intervals.

- Removal of existing falling debris hazards, if any, and repair of spall locations. Formation of spalls generally accelerates corrosion of nearby embedded reinforcement, resulting in an unpredictable accelerating propagation of visible deterioration. Locations of exposed, corroded reinforcement are generally isolated at this time but are expected to increase over time in the absence of such repairs.
- Partial-depth repair of concrete substructures at isolated bearing deterioration. Such locations of bearing deterioration do not appear to present a structural integrity hazard at this time, but unpredicted mechanical damage or preexisting conditions may result in additional deterioration over time.
- Sealing or resealing of bridge construction and expansion joints. Isolated regions of concentrated superstructure corrosion appear to be related almost entirely to leakage at the joints. While the asphalt topping appears to limit the moisture infiltration to the interior diaphragms, unsealed construction joints over the un-topped sidewalks appear to allow significant moisture infiltration, and resulting corrosion, at exterior diaphragms.

In conjunction with the above minimally invasive bridge maintenance strategies, the following strategies related to the load-posting are presented for consideration:

- We understand that prohibition of emergency vehicle use on the Austin Avenue Bridges may present a primary concern regarding bridge serviceability. Vehicles owned or operated by public, private, or volunteer fire departments are exempt from the load-posting currently in place at the bridges, per the Texas Transportation Code, Title 7, Subtitle E, Section 622.952. Therefore, no additional action is required for such vehicles to utilize the bridges.
- The results of the more in-depth field investigation, material evaluation, and structural modeling may warrant modification of the current load rating, depending upon the details of the existing analysis. Review or reevaluation of the bridge load rating as discussed previously may indicate that the in-place bridge is capable of supporting a standard HS 20 loading.
- Upon further investigation of the bridges, conditions noted as cause for the current rating, i.e. widespread pack rust of primary structural elements, may be less significant than originally concluded. Review or reevaluation of the bridge inspection rating may therefore be warranted, as discussed previously. However, such review or reevaluation is not TxDOT standard practice, so modification of the current bridge inspection rating is unlikely.
- Structural load testing may corroborate consideration of bridge capacity modification or load posting removal. Long-term monitoring can indicate long-term trends in gradually changing behavior or rapid notification of suddenly changing conditions or overstress. The observed absence of load-induced distress at the bridges, which could have occurred before the recent load posting, suggests that the in-place bridge capacity may be adequate for supporting a standard HS 20 loading.

Beyond the minimally invasive bridge maintenance and analysis strategies described above, the following strategies may warrant further consideration based upon the results of the advanced investigation and testing completed at the bridges:

- Replacement of the non-composite concrete deck, as recommended by A&F and Mr. Barnhart. Based on limited service life modeling, the existing bridge decks are likely to begin exhibiting significant carbonation-induced distress within the next 20 to 40 years. Bridge deck replacement with a composite deck could be achieved by adding shear connectors to the top flanges of the steel beams. Such would enhance the capacity of the bridges and appears to be suitable for phased construction, allowing the bridges to remain partially open to traffic. Removal of the existing deck would also facilitate the following advanced service life enhancements:
  - Superstructure coating (including girder top flanges), substructure repairs, and steel/lead bearing assembly replacement with neoprene bearing pads, as previously discussed.

  - Repair or replacement of any substantially deteriorated intermediate diaphragms and introduction of alternative deck-superstructure interface detailing to reduce the propensity for future haunch spalling or girder web corrosion.
- Life-cycle cost comparisons of additional mitigation and repair strategies, utilizing the completed advanced material testing and service life modeling, to better inform the above considerations. Functionality limitations, such as alignment, load restrictions, or traffic volume constriction, may factor into considering full bridge replacement, but full bridge replacement appears to be unnecessary within the predictable future, if only considering the condition of the bridges. In our experience, maintenance strategies listed above, or replacement of elements with the least remaining service life (decks), are typically more economical than full structural replacement in the long-term, when excluding such functionality limitations.

CLOSING

WJE's findings and recommendations are based on the observations and representative conditions at the time of our assessment. Other conditions may exist, or develop over time, which were not found during our initial investigation. WJE reserves the right to modify our findings should additional information become available. Our recommendations are conceptual and preliminary in nature and do not represent a design or specification for repairs. If requested, WJE is available and prepared to assist with further development of the conceptual recommendations and repairs described herein. This report was prepared for, on behalf of, and for the exclusive use of, Aguirre & Fields.

REFERENCES

1. AASHTO (2011). AASHTO Manual for Bridge Evaluation. 2nd ed. Washington, D.C.: AASHTO.
2. Broomfield, J. P. (2007). *Corrosion of Steel in Concrete*. New York: Taylor and Francis.
3. AASHTO (2010). *AASHTO LRFD Bridge Design Specifications*. 5th ed. Washington, D.C.: AASHTO.
4. Sagüés, A. (2003, October). Modeling the Effects of Corrosion on the Lifetime of Extended Reinforced Concrete Structures. *Corrosion*, 854-866.
5. Parrott, L. J. (1987). *A review of carbonation in reinforced concrete*. Wexham Springs, Slough: Cement and Concrete Association.
6. Tuutti, K. (1982). *Corrosion of Steel in Concrete*. Stockholm, Sweden: Swedish Cement and Concrete Research Institute.
7. Alonso, C., Andrade, C., Rodriguez, J., & Diez, J. M. (1998). Factors controlling cracking of concrete affected by reinforcement corrosion. *Materials and Structures*, 31, 435-441.
8. Parrott, P. J. (1994). Design for Avoiding Damage Due to Carbonation-Induced Corrosion. *ACI Special Publication*, 283-298.
9. Bamforth, P. (2004). *Enhancing reinforced concrete durability: Guidance on selecting measures for minimising risk of corrosion of reinforcement in concrete, Concrete Society Technical Report No. 61*. Surrey, UK: The Concrete Society.
10. RILEM TC 130-CSL (1996). *Durability design of concrete structures, RILEM Report Series 14*. ed. A. Sarja and E. Vesikari. London: E&FN Spon.

TABLES

Table 1. GPR Cover Depth Survey Summary

Elements (*bar type*)	Cover Depth Determined with GPR	
	Average (in.)	Minimum (in.)
Deck Soffit (*primary*)	1-1/8	3/4
Bents/Piers (*stirrups*)	2-1/2	1-1/2
Abutments (*stirrups*)	2-1/4	1-3/8

Table 2. Carbonation Depth Survey Summary

Elements	Average Carbonation Depth (in.)		
	Cores	Drilled	Average
Deck Soffit	1-1/16	3/4	15/16
Substructure Elements	5/16	5/16	5/16

Table 3. Core Testing Summary

Core ID	Core Description	Testing Schedule			
		Strength	Carbonation	Chlorides	Petrography
1	North, Bent 2, Stained		X	X	
2	North, Bent 2, Unstained		X	X	
3	North, Span 7, Sidewalk Top		X	X	
4	North, Bent 4, Stained		X	X	
5	South, Span 1, Deck	X (5,100 psi)			
6	South, Span 7, Deck		X	X	
7	North, Span 1, Deck	X (4,790 psi)			
8	North, Span 7, Deck		X	X	X
9	South, Bent 2, Stained		X	X	
10	South, Bent 2, Unstained		X	X	
11	South, Bent 5, Stained	X (6,500 psi)			
12	South, Bent 6, Unstained	X (7,000 psi)			
13	South, Abutment 8, Top		X	X	
14	North, Pier 5, Unstained			X	X

Table 4. Acid-soluble Chloride Summary

Core ID	Maximum Chloride Test Depth Range (inches)	Acid-soluble Chlorides (% by concrete mass)		
		Surface (near surface)	Intermediate (1/2 of cover)	Reinforcement (cover depth)
1	2 to 2-1/2	0.029	0.029	0.022
2	2 to 2-1/2	0.036	0.015	0.007
3	2 to 2-1/2	0.048	0.024	0.018
4	2 to 2-1/2	0.035	0.038	0.019
6	1-1/4 to 1-1/2	0.027	0.021	0.021
8	1-1/4 to 1-1/2	0.044	0.039	0.027
9	2 to 2-1/2	0.024	0.007	0.006
10	2 to 2-1/2	0.039	0.009	0.006
13	2 to 2-1/2	0.031	0.012	0.006
14	2 to 2-1/2	0.014	0.005	0.004

Table 5. Service Life Model Input Parameters

Variable	Units	Distribution Type	Parameters	Notes
Cover	in.	Lognormal	μ: 0.070 σ: 0.170	Mean: 1.09 N: 39
Carbonation Rate Constant	in./year$^{1/2}$	Lognormal	μ: -2.273 σ: 0.313	Mean: 0.93 N: 11
Corrosion Rate (90% RH)	mils/year	Normal	μ: 0.02 σ: 0.07	COV: 35% Assumed value
Corrosion Rate (70% RH)	mils/year	Normal	μ: 0.04 σ: 0.014	COV: 35% Assumed value
Critical Section Loss	mils	Constant	3 mils	Assumed value

FIGURES

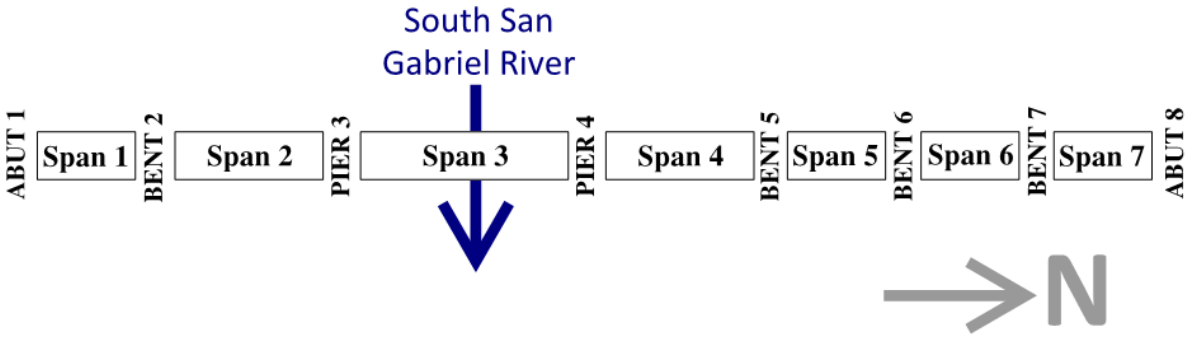

Figure 1. Schematic orientation of South Austin Avenue Bridge; Span 3 includes a 56-foot suspended span between 14-1/2-foot cantilevered extensions from Spans 2 and 4.

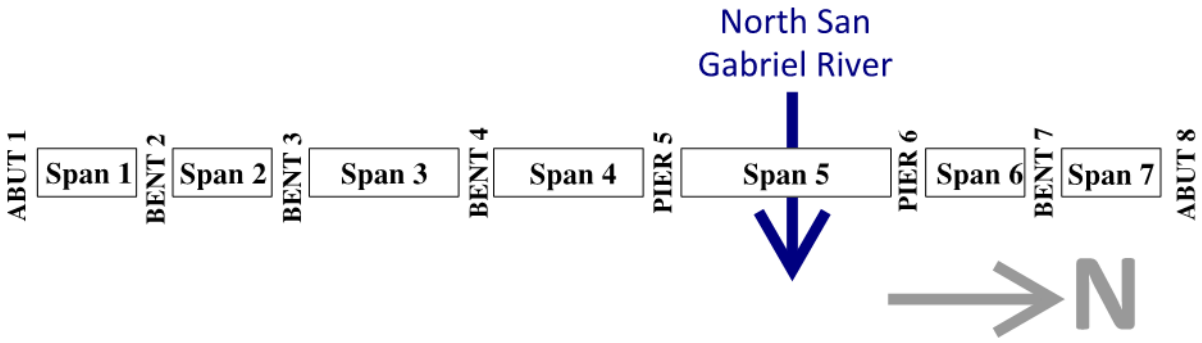

Figure 2. Schematic orientation of North Austin Avenue Bridge; Span 5 includes a 56-foot suspended span between 14-1/2-foot cantilevered extensions from Spans 4 and 6.

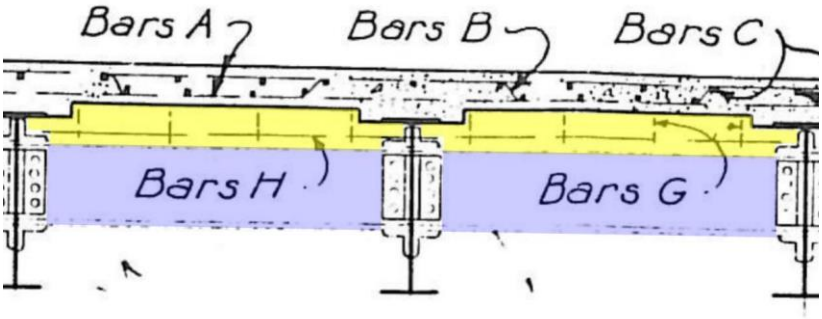

Figure 3. Elevation view of typical diaphragm detailing, with concrete and typical reinforcing highlighted in yellow and steel diaphragms shaded in blue.

Figure 4. Typical diaphragm detailing (south end of North Bridge shown).

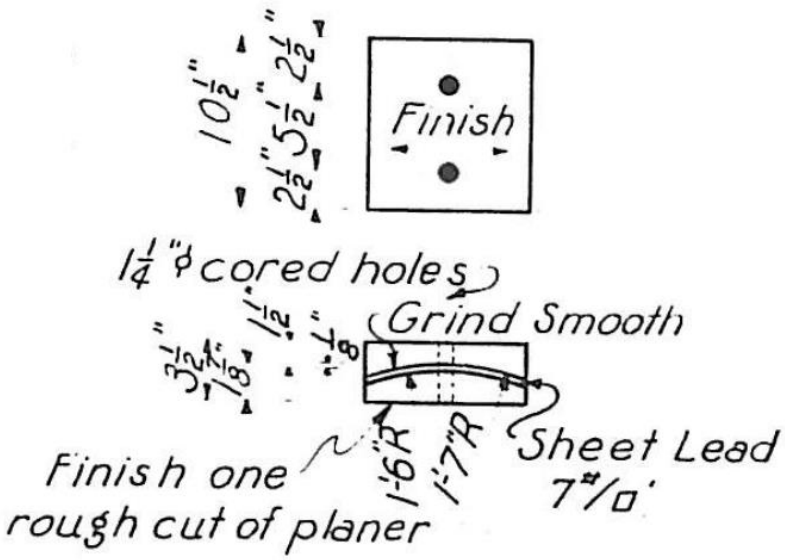

Figure 5. Typical steel ball-and-socket bearing detail, with lead sheet between steel plates.

Figure 6. Typical bearing detail (south end of South Bridge shown).

Figure 7. Use of 50-foot articulating boom lift to conduct non-destructive testing at North Bridge Pier 5.

Figure 8. Typical movement at corner of North Bridge (southwest corner shown), with spalling along unreinforced haunch chamfer.

Figure 9. Typical gap at corner of North Bridge (southwest corner shown), with lack of apparent corrosion on girder top flange.

Figure 10. Typical, isolated deck soffit spall with two exposed, corroded bars (east side of South Bridge Span 3 shown).

Figure 11. Typical chamfered haunch spall, with no visible reinforcement.

Figure 12. Typical cracking of diaphragm concrete, originating at reentrant corner created by girder top flange. Interior diaphragm with minimal corrosion shown.

Figure 13. Typical leakage beneath expansion joints, with evidence of persistent moisture staining near exterior bent columns.

Figure 14. Typical isolated spall at base of pedestrian rail post, with exposed, corroded post base (northeast side of North Bridge shown).

Figure 15. Moderate corrosion pitting of girder web at diaphragm connection, where diaphragm concrete is cast flush with steel (web section loss of approximately 1/8 inch). Interior face of outermost girder shown.

Figure 16. Typical pack rust formation at diaphragm top flange, with flange tip section loss.

Figure 17. Corrosion of outermost bearing assembly, with deterioration/protrusion of lead sheet. Southeast corner of South Bridge shown.

Figure 18. Pack rust formation at outermost bearing exposed to prolonged sidewalk drainage (east side of South Bridge Bent 2 shown).

Figure 19. Large spall at South Bridge Bent 2.

Figure 20. Spall debris from South Bridge Bent 2 spall, exhibiting approximately 2 inches of concrete cover to the reinforcement, based on indentation in debris.

Figure 21. Delamination (insipient spall) at South Bridge Abutment 1, highlighted with red dashed line.

Figure 22. Typical isolated spall at abutment back wall, with exposed, corroded reinforcement (South Bridge Abutment 1 shown).

Figure 23. Isolated bent cap soffit spall (North Bridge Bent 2 shown).

Figure 24. Scour at east end of South Bridge Pier 3, with concentrated water flow due to boulders in San Gabriel River.

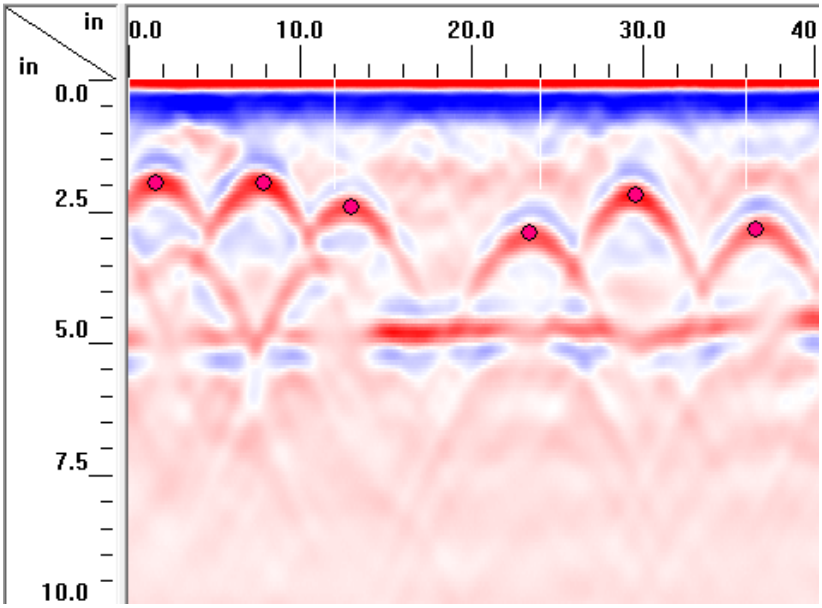

Figure 25. Example recorded scan of reinforcement in bent column, with red markers indicating cover depths to reinforcement.

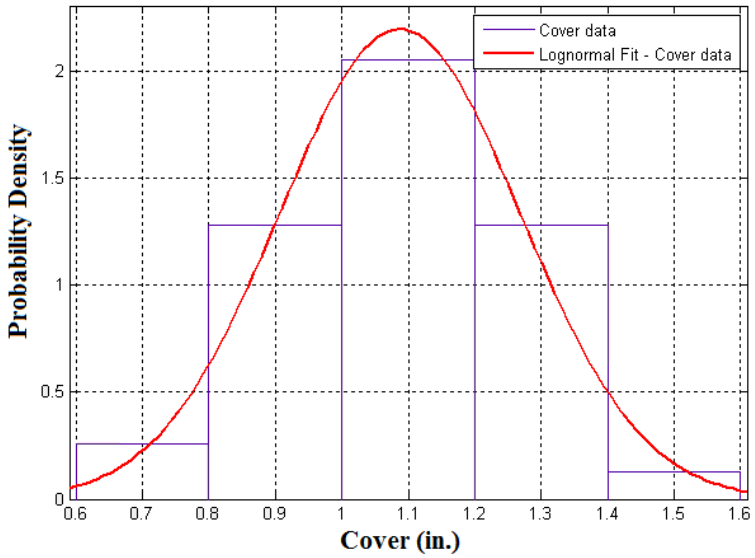

Figure 26. Distribution of deck soffit cover measurements obtained using GPR equipment.

Figure 27. Typical carbonation testing using phenolphthalein solution (pink hue indicates high pH, while lack of color indicates carbonation).

Figure 28. Coring equipment used to obtain 3-3/4-inch cores through Austin Avenue Bridge decks (North Bridge Span 1 shown).

Figure 29. Core removed from South Bridge Bent 5 west face, from location exhibiting minimal surface staining (Core 11).

Figure 30. Collection of 14 3-3/4-inch cores obtained from the Austin Avenue Bridges.

Figure 31. Fractured Core 8, in which the carbonation depth (non-pink region) has not reached the reinforcement, and reinforcement exhibits no corrosion.

Figure 32. Core 6, with apparent carbonation beyond depth of embedded No. 5 reinforcement.

Figure 33. Fractured Core 6, in which reinforcement only exhibits surface corrosion where carbonation depth exceeds concrete cover (non-pink region in middle of core).

Figure 34. Laboratory investigation of carbonation depth, utilizing phenolphthalein carbonation indicator.

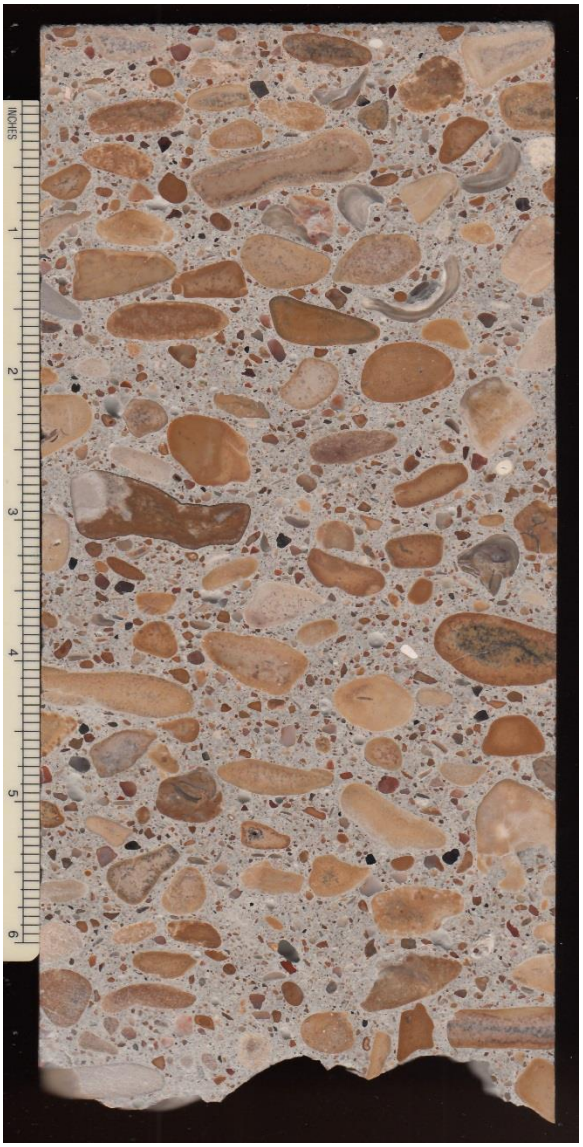

Figure 35. Polished surface of Core 14, scanned for petrographic analysis (outer surface of core at top of scan).

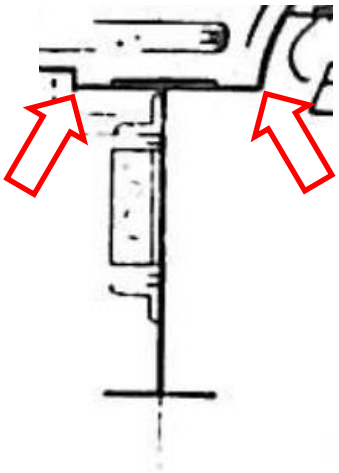

Figure 36. Unreinforced regions of haunch chamfers (arrows), susceptible to spalling due to detailing.

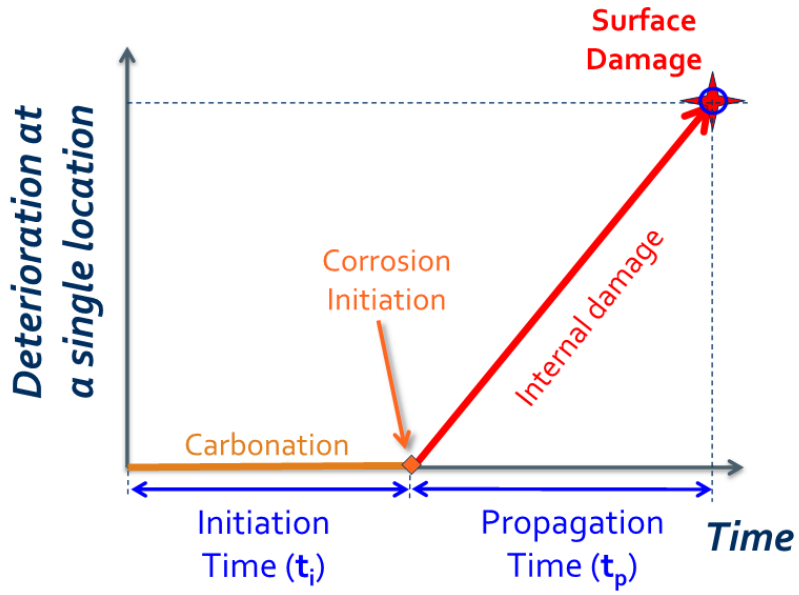

Figure 37. Corrosion sequence (adapted from Tuutti 1982 [6]).

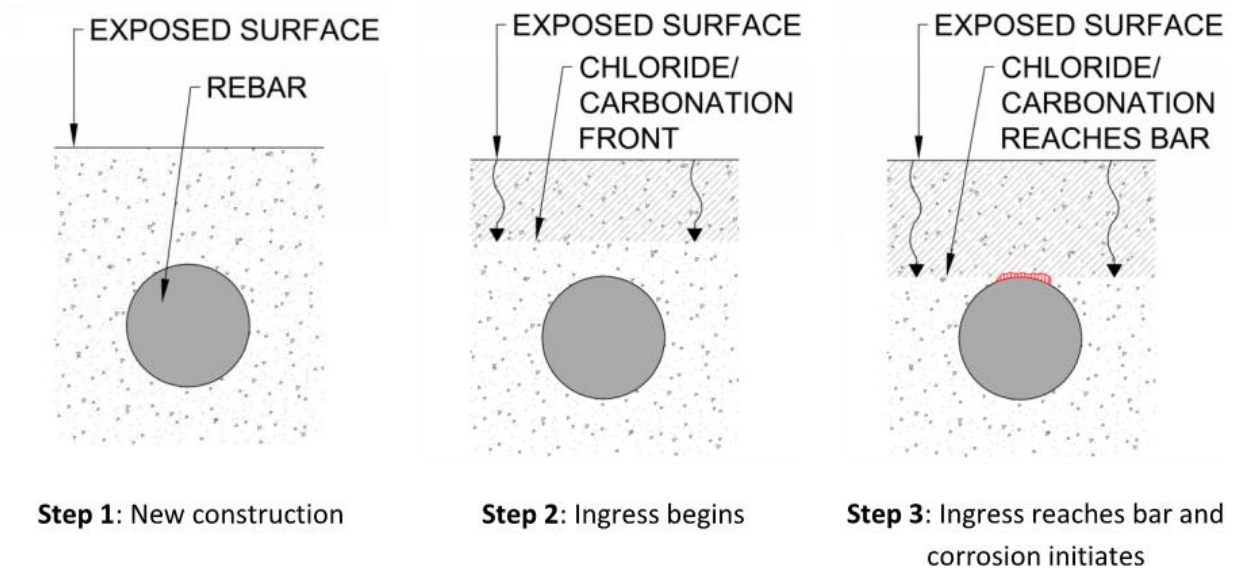

Figure 38. Illustration of general corrosion sequence.

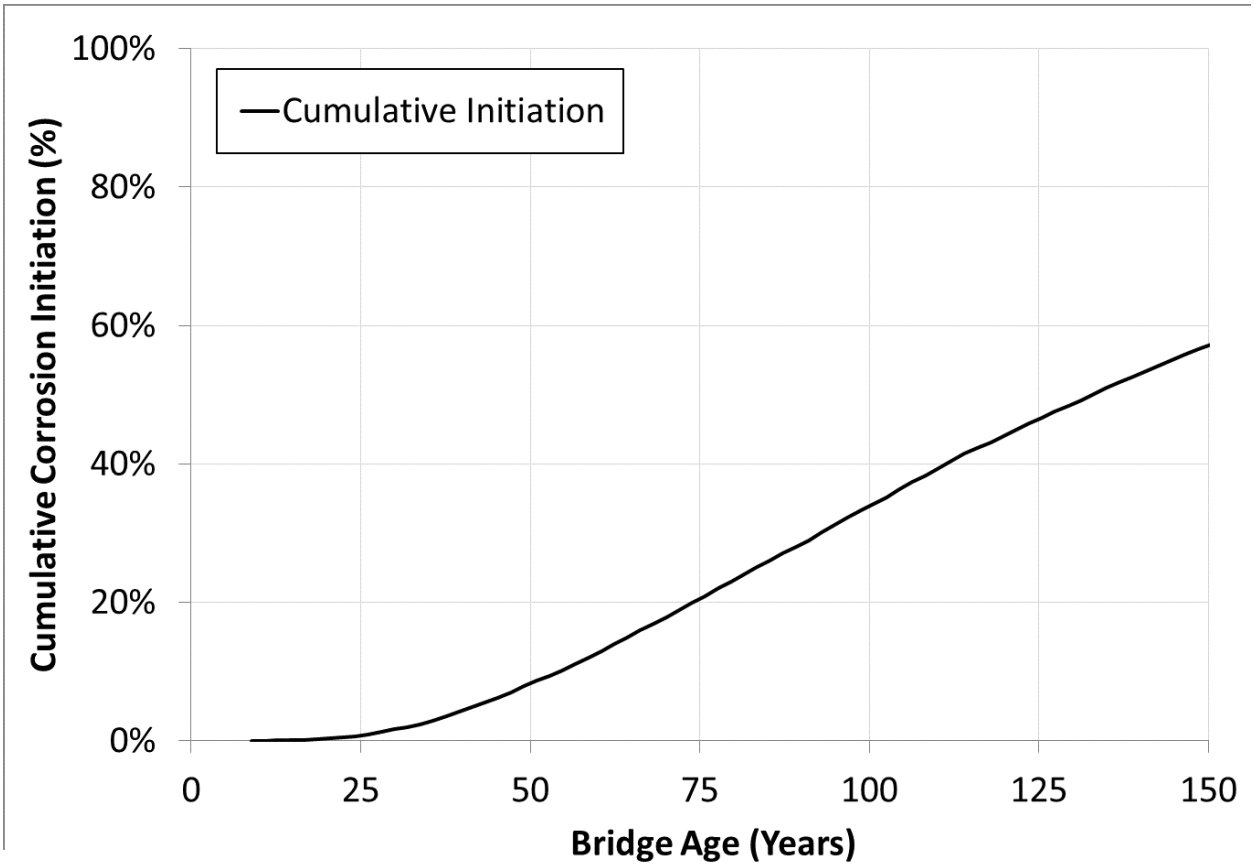

Figure 39. Cumulative estimate of carbonation-induced corrosion initiation, representing percentage of reinforcement likely embedded in carbonated concrete (approximately 20 percent at age = 75 years).

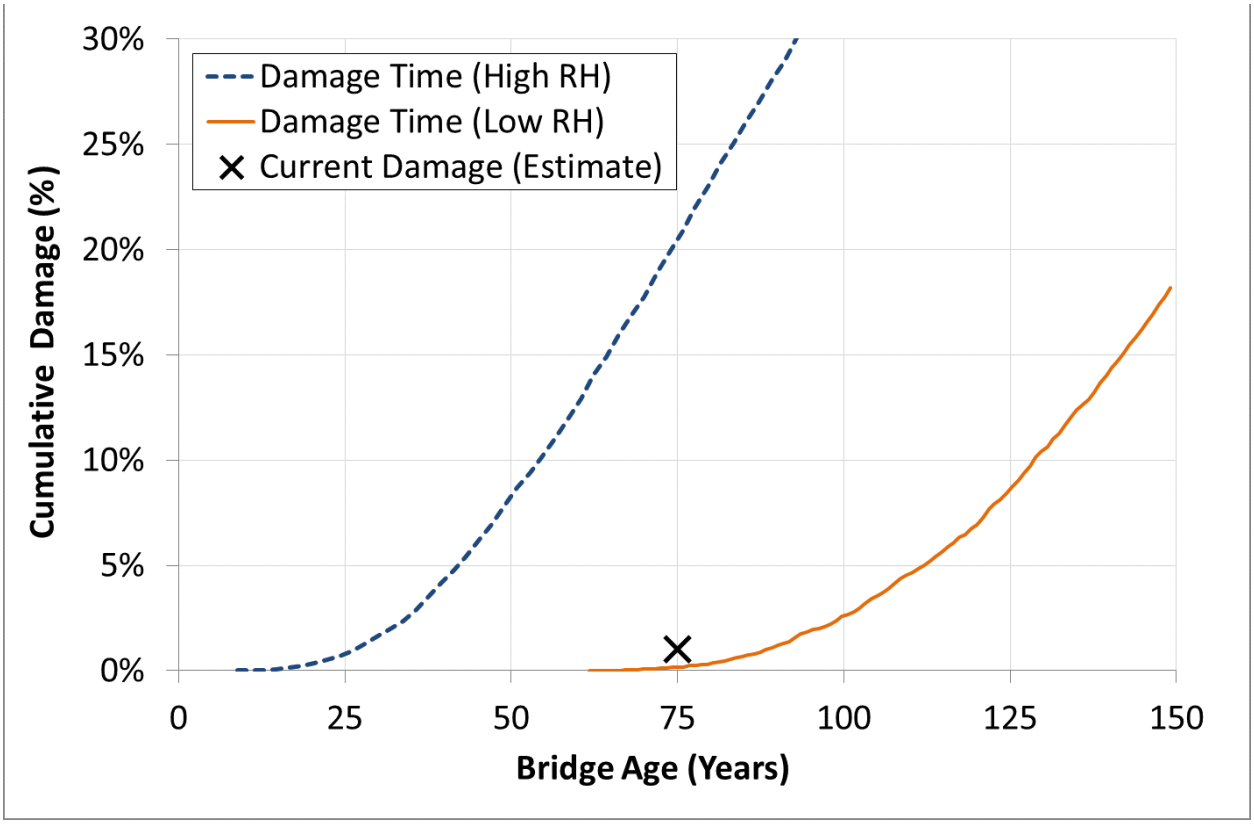

Figure 40. Estimates of cumulative visible soffit damage, based on corrosion rates from the literature.